ADVANCED MATERIALS TECHNOLOGIES
www.advmattechnol.de

Additively Manufactured Ferroelectric Particulate Composites for Antimicrobial Applications

Zois Michail Tsikriteas, Rachel A. Heylen, Swati Jindal, Elena Mancuso, Zihe Li, and Hamideh Khanbareh**

A polarized ferroelectric material can initiate the micro-electrolysis of water molecules which leads to the formation of reactive oxygen species (ROS) in an aqueous solution resulting in selective bacteria killing. This study presents the fabrication, characterization, and antimicrobial performance of poled ferroelectric particulate composites. Barium calcium zirconate titanate (BCZT) micropowder is synthesized by a solid-state reaction and mechanically mixed with polycaprolactone (PCL) to be subsequently fed into the 3D bioprinter for the fabrication of porous PCL-BCZT structures at four different ceramic loadings (0, 10, 20, 30 wt%). For the examination of material's capacity to handle extremely high contamination, the composites are exposed to a high inoculum of bacteria (*Escherichia coli* ATCC 25922) ≈70% of *E. coli* degradation is recorded at the end of 15 min without any external intervention. The surface selective bacterial degradation can be attributed to the generated reactive oxygen species, the large surface area of the porous samples and polymer matrix's hydrophobic nature, behavior which can be reflected in the composites with 30 wt% of BCZT loading exhibiting the best antimicrobial performance among the other state-of-the-art ferroelectrics. Overall, these results indicate that the poled composites have a great potential as antimicrobial materials and surfaces.

1. Introduction

Since they first began to exist millions of years ago, microorganisms, which include bacteria, viruses, fungus, algae, and many other living species, have had an extraordinary impact on practically every area of human life, both beneficial and harmful; for example, they cause serious infections, such as sepsis.[1] Biomaterials used as medical implants have come to the forefront in the healthcare sector. The usage of implants as heart valves, stents,[2] and tissue-like replacements[3] that can enhance the tissue damage and repair under challenging conditions have significantly increased over the past years. However, these materials are not devoid of surface bio-contaminations posing a significant health risk to patients and costing healthcare systems with millions of dollars.[4] Since the discovery of penicillin, persistent efforts have been made to cure and prevent microbiological contaminations.[5] Drug-resistant bacteria, however, present a formidable problem for sanitation and healthcare adding new challenges to the research community.[6] Although the emergence of antimicrobial resistance (AMR) in microorganisms is a natural process, AMR has been influenced by the misuse and overuse of antibiotics in health care, agriculture, and the environment.[7] Particularly, within the healthcare sector AMR compromises the capability to treat infectious diseases. According to Grand view Research, around 2.8 million cases of AMR occur every year in the United States. In addition to this, the United States Pharmacopeial Convention estimated that AMR caused about 700 000 deaths per year worldwide. Moreover, this number is expected to reach 10 million per year by 2050, if diagnosis and treatment of microbial infections are not properly managed.[8] Hence, the development of novel antimicrobials or alternatives is a prime example of unmet medical need. The majority of the current strategies to prevent microbial growth on surface are mainly based either on contact killing of bacterial cells, antibiotics, and inorganic metal ion release from the surface.[9] However, these existing methods come with certain inherent dangers, such as bacterial resistance to antibiotics, high cytotoxicity of inorganic salts, and metal ion accumulation on the human body.[10] In light of the worldwide position about AMR, it is of a great importance

Z. M. Tsikriteas, Z. Li, H. Khanbareh
Materials and Structures Research Centre
Department of Mechanical Engineering
University of Bath
Claverton Down, BA2 7AY Bath, UK
E-mail: zmt25@bath.ac.uk; hk497@bath.ac.uk
R. A. Heylen
Department of Chemistry
University of Bath
BA2 7AY Bath, UK
S. Jindal
School of Mechanical Engineering
University of Leeds
LS2 9JT Leeds, UK
E. Mancuso
R&D Division
Engineering Ingegneria Informatica S.P.A.
Piazzale dell'Agricoltura 24, 00144 Rome, Italy
The ORCID identification number(s) for the author(s) of this article can be found under https://doi.org/10.1002/admt.202202127.

DOI: 10.1002/admt.202202127

to discover new sustainable methods for the prevention of surface bio-contaminations.

Many types of cells and single-cell organisms like bacteria have been found to be sensitive to electric stimulation.[11,12] Thus, there has been an increasing interest from the research community to further exploit the use of ferroelectrics for biomedical applications. Ferroelectric materials' unique ability to convert mechanical deformation and thermal fluctuations into an electric signal and vice versa is used in a wide range of applications, from ultrasound devices to mobile phone buzzers and infrared sensors. It is also well established that piezoelectric or other forms of electrical stimulation can promotes tissue repair or regeneration by influencing the behavior of the target tissues, by altering the transmembrane potential and triggering the propagation of action potentials in neurons.[3,13] It is worth noting that the specific mechanisms by which electrical stimulation promotes tissue formation may vary depending on the type of tissue, the type and intensity of the electrical stimulus, and other factors.[14] In the case of bacterial degradation, the main idea is that the remnant polarization can initiate electrochemical surface reactions resulting in ROS production. There are three main mechanisms with which ferroelectrics can induce or modify electrochemical reactions: 1) catalysis by electric field,[15] 2) mediated (piezo/pyro) catalysis,[13,16] and 3) photoelectrolysis.[17]

Ferroelectrics with high piezoelectric performance and biocompatibility, such as barium calcium zirconate titanate $0.5Ba(Zr_{0.2}Ti_{0.8})O_3–0.5(Ba_{0.7}Ca_{0.3})TiO_3$ seem to be suitable candidates for these applications. Despite the promising properties of ferroelectrics, there are inherent limitations, such as poor processability as well as brittleness, that make their application confined. In order to overcome these drawbacks, particularly for applications where a certain level of mechanical performance is needed, the use of ferroelectrics in the particulate form and for the development of composite materials has revealed as a promising approach.[18,19] In such a way the single phase complements each other's strengths and weaknesses, contributing to overcome the limitations deriving from the use of one material only. In addition to this, the processing of particulate-based composites through additive manufacturing (AM) technology has gained great attention in the last decade, in order to produce customized 3D structures in a variety of geometries and for different applications (i.e., aerospace, automotive, clean technology as well as the biomedical field).[3,20,21] Based on the promising findings of a recent study from the authors,[3] in this work green chemistry basic principles were followed by using an environmentally friendly AM technology.

Specifically, a solvent-free extrusion-based 3D printing approach was used in order to process a composite based on a polymeric matrix of thermoplastic polycaprolactone and a ferroelectric particulate phase at various concentrations. PCL was selected for its widely documented processability, low melting temperature, biodegradability, biocompatibility, mechanical resistance, relatively low cost, and its extensive adoption in healthcare applications.[22,23] Attenuated total reflectance Fourier transform infrared spectroscopy (ATR-FTIR) was performed on the printed specimens. The microstructure of the composites was studied via scanning electron microscopy and in all cases, high inner consistencies and fine dispersions were detected. The thermal behavior of the 3D printed composites, upon heating, was investigated via thermogravimetric analysis (TGA) while the electrical response of the composite specimens was examined by means of impedance spectroscopy at three different temperatures (25, 36.6, and 50 °C) in a wide frequency range ($0.1–10^4$ Hz). A poling study was performed using a Corona poling set-up and the effect of time, temperature, and the electric field strength on the poling efficiency of the composites was studied. Finally, the antimicrobial performance of the poled ferroelectric particulate composites was assessed by exposing them to a high inoculum of bacteria (*E. coli* ATCC 25922).

2. Results and Discussion

Figure 1 shows the scanning electron microscopy image and the X-ray diffraction pattern of the synthesized BCZT powder. Good crystallization of the powder can be observed as the peaks are strong with small width at half maximum (FWHM). In addition, there are not indications of other structural phases or any splitting or super-lattice reflections in the diffractogram matching the tetragonal $BaTiO_3$ structure with the P4mm space group according to the JCPDS card 05-0626. The corresponding (hkl) miller indices have annotated in the figure. The Coulomb repulsion between the 3d electrons of Ti^{4+}/Zr^{4+} ions and the 2p electrons of O^{2-} ions caused the distorted crystal structure in the $BaTiO_3$-based ceramic, leading to a stable tetragonal structure. The splitting of the (200) peak

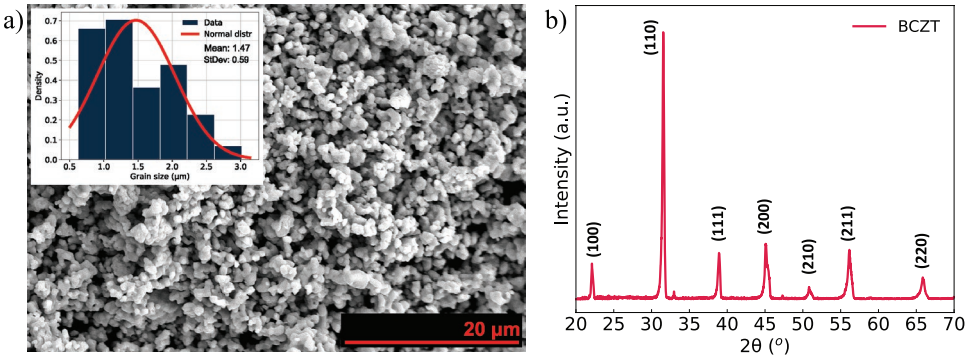

Figure 1. a) SEM micrograph and particle size analysis of the synthesized BCZT powder. b) XRD spectrum of the synthesized BCZT powder.

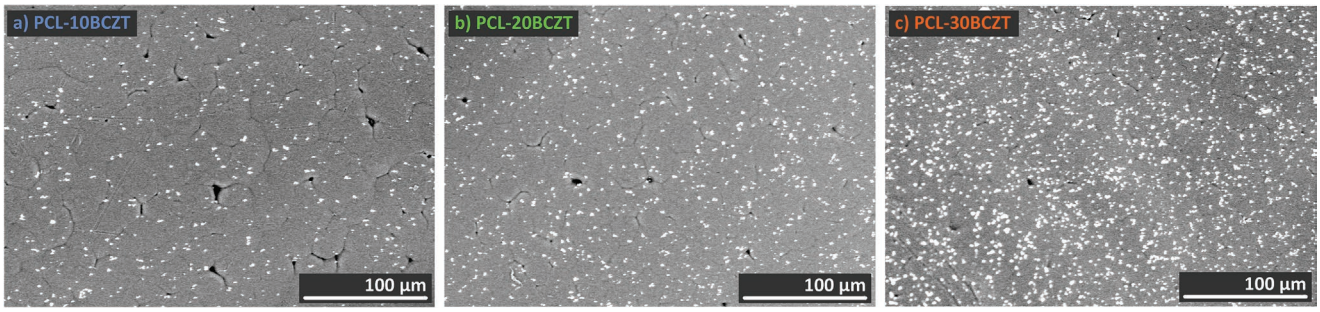

Figure 2. SEM morphological evaluation of the three printed ferroelectric composites at different concentrations: a) 10 wt% BCZT, b) 20 wt% BCZT, and c) 30 wt% BCZT.

of pure BCZT into (002) and (200) peaks in the 2θ range of 44–46° at room temperature corresponds to the diffusion of Ca^{2+} (A-site) and Zr^{4+} (B-site) ions into Ba^{2+} (A-site) and Ti^{4+} (B-site) respectively, confirming the formation of a tetragonal or tetragonal-dominant phase.[24] After calcination, the BCZT powder exhibited an irregular shape morphology with an average particle size of 1.47 µm.

Scanning electron micrographs (SEM) of the additively manufactured composites in the three different concentrations of BCZT are shown in **Figure 2**. A homogenous distribution of BCZT microparticles is observed in the PCL matrix in all cases.

Bacterial adhesion can be inhibited by the surface characteristics of a material, such as its topography, chemistry, and roughness.[25] In order to evaluate the surface characteristics of the 3d printed samples, 3D topographic images were obtained and are shown in **Figure 3**. The images shows that the 3d printed samples' design and the interconnected porosity matches the computer-aided design to a large extend demonstrating the

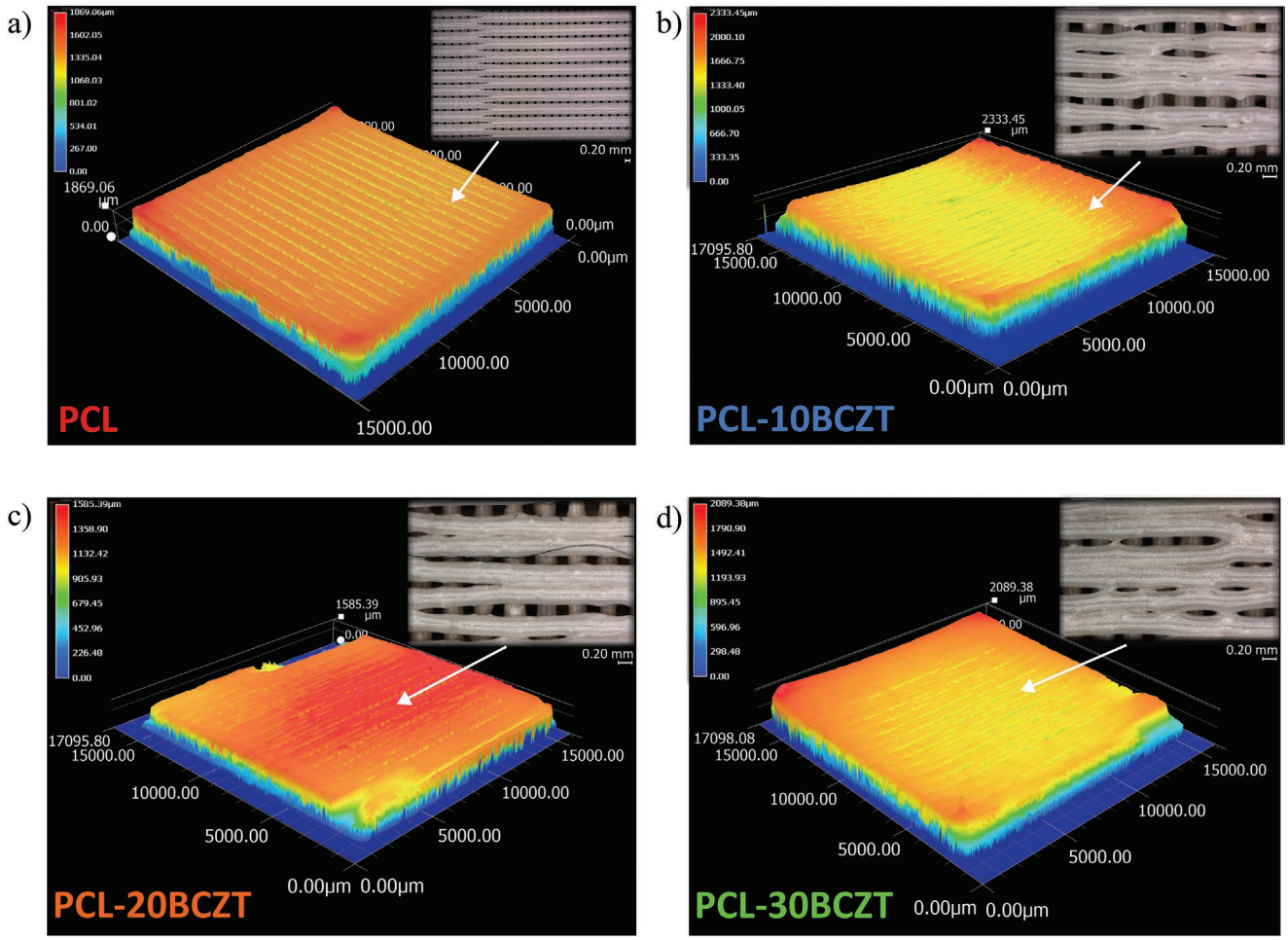

Figure 3. Three-dimensional images of the printed samples.

Table 1. Morphological characteristics of the 3d printed samples.

Sample	Width [mm]	Length [mm]	Height [mm]	Weight [g]	Density [g cm^{-3}]	Porosity [%]	Strand diameter [mm]	Sa [µm]	Sz [µm]
PCL	15.39	15.38	1.38	0.27	1.135	26.5	0.28	103.72	1459.69
PCL–10 wt% BCZT	15.27	15.28	1.47	0.28	1.242	32.9	0.29	152.65	1877.03
PCL–20 wt% BCZT	15.52	15.5	1.52	0.36	1.36	27.1	0.32	129.87	1286.46
PCL–30 wt% BCZT	15.42	15.43	1.5	0.39	1.5	26.1	0.34	98.66	1326.52

effectiveness of the printing process. However, it is evident that the printing of the samples becomes more challenging with the increase of the inorganic phase concentration. This can be confirmed by the average strand diameter data (**Table 1**) where the average diameter increases with the increase of the BCZT concentration affecting the print quality and as a result the porosity of the samples.

The surface arithmetical mean height (Sa) and maximum surface height (Sz) extracted from the three-dimensional topographic observations are presented in Table 1. Surface roughness can affect bacterial adhesion in a number of factors. Bacteria can use the rougher surface area for better anchoring on the surface since rougher surfaces tend to have a higher number of sites for bacterial adhesion, which can lead to increased bacterial adhesion. Consequently, smoother surfaces may be more resistant to bacteria attachment. Additionally, surface roughness can influence the mechanical properties of a material, such as its strength and stiffness, which can also affect bacterial adhesion.[26]

ATR-FTIR analysis was used on the PCL as well as the 3D printed composites in order to confirm the presence of BCZT in the composites. As reported in **Figure 4**, the characteristic bands of PCL can be seen in all the 3D printed composites. More specifically, the characteristic peaks at 2943 and 2865 cm^{-1} corresponding to the typical C–H functional group in CH_2, the C = O carbonyl group at 1720 cm^{-1}, the CH_2 deformation band from 1165 to 1468 cm^{-1} and the backbone C–O and C–C stretching of the crystalline phase at 1293 cm^{-1} are detected. Additionally, the symmetric and the asymmetric band at 1239, 1164, 1107, and 1047 cm^{-1} were also observed.[27] On the other hand, the characteristic bands of barium calcium zirconate titanate we only spotted in the composite systems. More specifically the Ti–O stretching vibration peak appeared at 559 cm^{-1}.[28] This confirms the presence of the ferroelectric ceramic phase in the systems. In addition, the intensity of the peak increases with the increase of the ceramic phase. This agrees well with the scanning electron microscopy SEM images and is another indication of good dispersion of the ferroelectric ceramic filler and successful extraction of the filament.

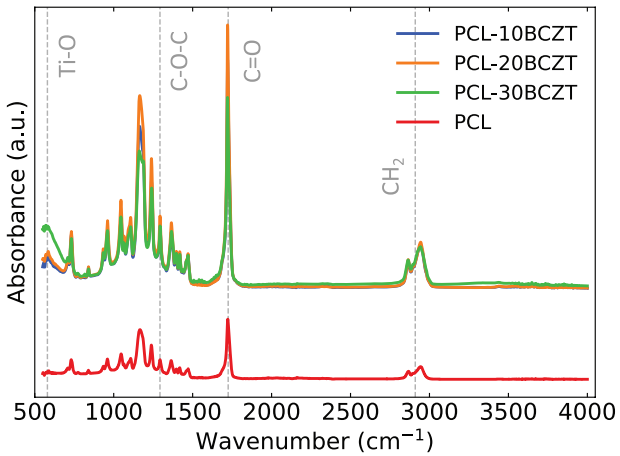

Figure 4. FTIR spectra comparing PCL-10BCZT (blue), PCL-20BCZT (orange), and PCL-30BCZT (green) with the polymer matrix (red).

TGA was performed to determine the chemical stability of the composites at elevated temperatures as shown in **Figure 5**. For each sample, there was a single-step degradation and a significant mass loss. According to Figure 5, the melting of the powder blend starts happening at 55 °C, indicating that the temperature must not exceed this value during the electrical or poling studies in order to ensure uniform geometry and consistent structural integrity with high fidelity to the computer-aided design (CAD) model dimensions. The main structural decomposition started at a temperature above 250 °C, thus confirming the stability of all the compositions during the printing process. The 50% weight loss occurs at ≈385, ≈390, ≈400, and ≈411 °C for the PCL, 10, 20, and 30 wt% respectively. After 510 °C the polycaprolactone was completely decomposed. The weight loss up to this temperature can be ascribed to the three-step degradation process of PCL which decomposes to carbon dioxide, water, carbon monoxide and short-chain carboxylic acids.[29] When the concentration of the BCZT increased the weight loss of the composites decreased. Also, as shown by the TGA first derivatives curves, which indicate that the presence of the inorganic ferroelectric phases contributed to a small shift in the maximum peaks toward higher temperatures, indicating the effect of the BCZT particles in delaying the material's degradation rate.[30]

Figure 6 shows the dielectric permittivity, alternating current (AC) conductivity and the dielectric losses of the 3D printed ferroelectric composite in the frequency range of 0.1–10^4 Hz at room temperature (≈25 °C), human body temperature (≈37 °C) and 50 °C temperature was chosen for the poling study. As it can be seen in Figure 6a, the permittivity of the composites increases with the increase of content filler and the increase of the temperature. The permittivity values decrease with the increasing frequency. This can be attributed to the inadequacy of the dipoles to follow the alternating electric field in the higher frequencies. A similar pattern is also observed in the losses of the 3D printed composites, Figure 6b. However, the tanδ values remain low across the whole measured frequency range indicating good quality dielectric materials. As expected, the dielectric loss spectrum does not indicate the presence of relaxation mechanisms in the tested temperature range since

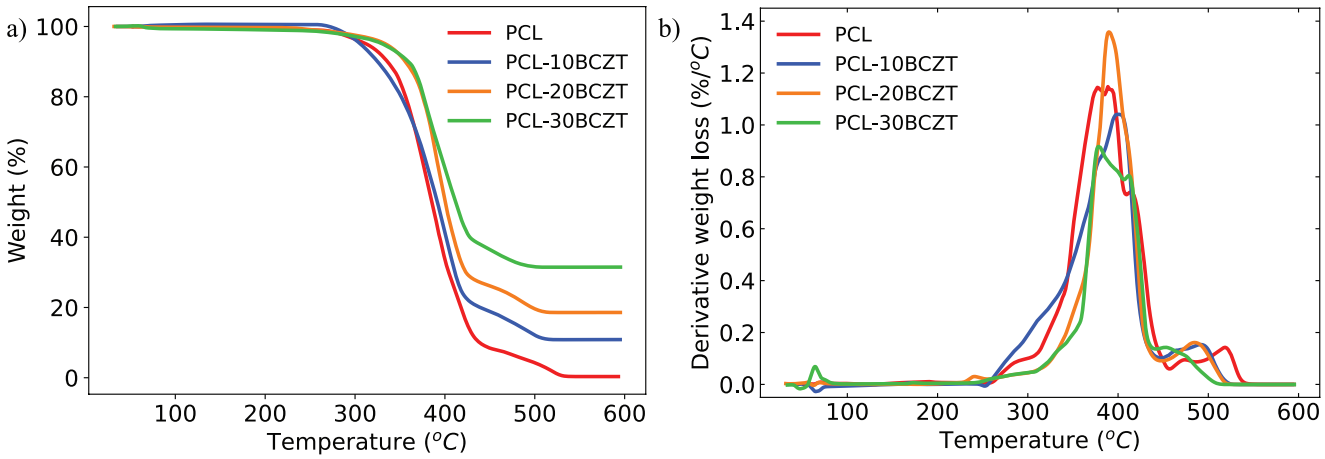

Figure 5. Thermogravimetric analysis of the samples after extrusion: a) TGA thermographs indicating the remaining mass for each tested sample, b) TGA first derivative curves of PCL-10BCZT, PCL-20BCZT, and PCL-30BCZT.

the main relaxation phenomena attributed to the polymer matrix appear at lower or higher temperatures (PCL-BCZT composites melting point ≈55 °C, Maxwell–Wagner–Sillars (MWS) crystalline amorphous phase ≈0 °C, α-relaxation ≈–60 °C, β-relaxation ≈–110 °C, and γ-relaxation ≈–150 °C[31]). The measured AC conductivity at the three tested temperatures

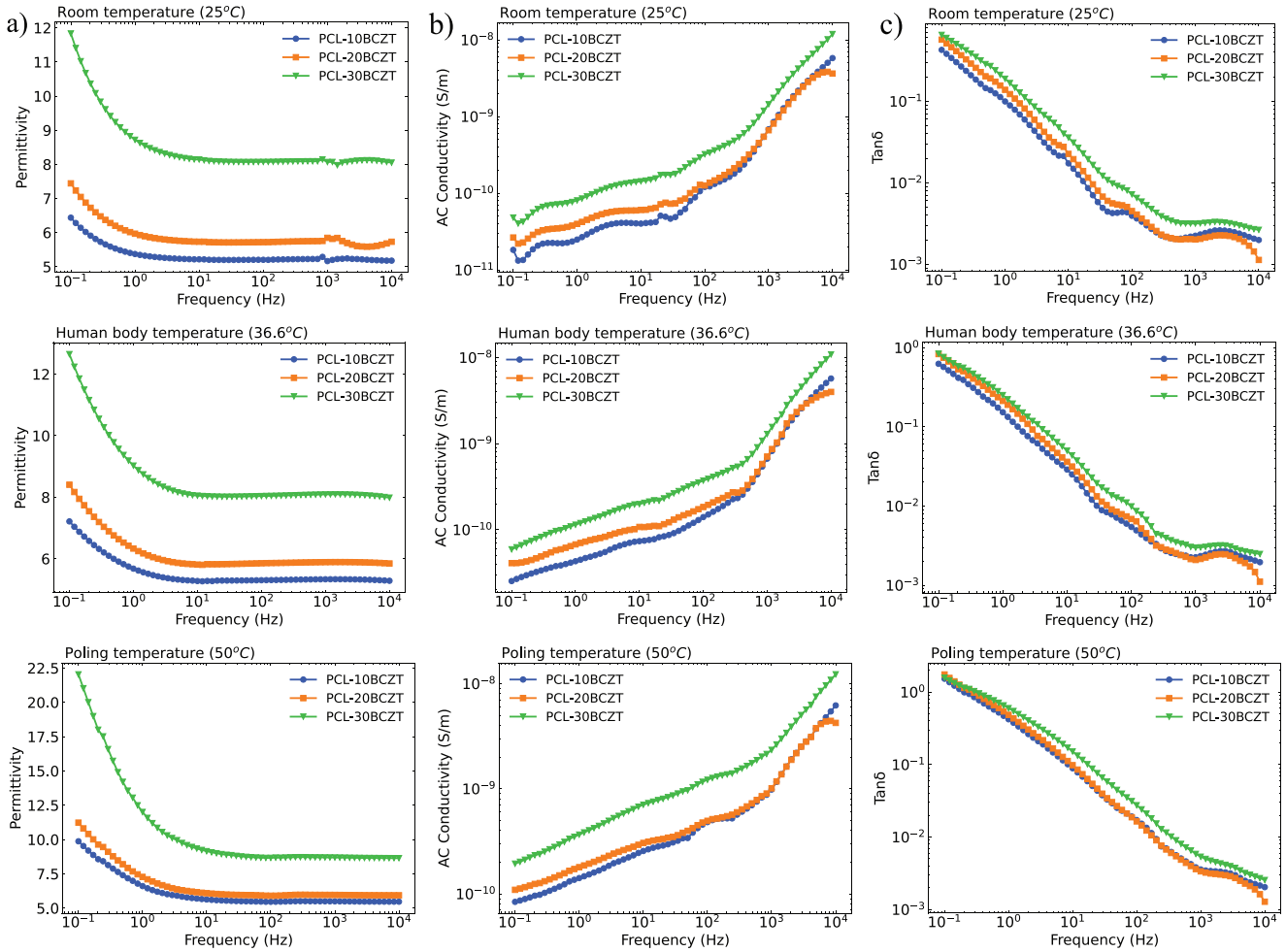

Figure 6. Dielectric response of the 3d printed ferroelectric composites as a function of frequency at three different temperatures: a) Real part of dielectric permittivity, b) AC Conductivity (S m^{-1}), and c) Loss tangent (tanδ).

Table 2. Dielectric and piezoelectric properties of the samples.

Sample	Dielectric permittivity measured at 1 kHz	Yamada model ε_{eff}	tanδ	d_{33} [pC N^{-1}]	g_{33} [mVm N^{-1}]	Yamada model $d_{33\,eff}$
PCL	4.4	–	0.01	–	–	–
Bulk BCZT pellets	2676.5	–	0.0364	400.5	16.9	–
10 wt% BCZT	5.2	5.37	0.0022	0.21	4.6	0.16
20 wt% BCZT	5.7	6.6	0.0019	0.36	7.1	0.4
30 wt% BCZT	8.1	8.15	0.0031	1.13	15.8	0.74

shows the presence of flat, dispersive, and linear regions as a function of frequency which is in agreement with the reported behavior for PCL in literature[32] and similarly manufactured composite systems with similar components.[3]

For the evaluation of the dielectric properties of the 3d printed composites the measured permittivity values were compared with data calculated using Yamada model which is a model specified for piezoelectric materials and most of the times shows a close matching with the dielectric constant of piezoelectric composites. The equation for this model is given below:

$$\varepsilon_{eff} = \varepsilon_{PCL}\left[1+\frac{nV_f(\varepsilon_{BCZT}-\varepsilon_{PCL})}{n\varepsilon_{PCL}+(1-V_f)(\varepsilon_{BCZT}-\varepsilon_{PCL})}\right] \quad (1)$$

where ε_{BCZT} is the relative permittivity of BCZT, ε_{PCL} is the relative permittivity of PCL, V_f is the volume fraction of ceramic filler, and n is the parameter attributed to the shape factor.[33] The experimental permittivity data are in good agreement with Yamada model (**Table 2**). The shape parameter n was calculated by fitting the experimental data and estimated to be around 2.

A custom-made corona discharge poling single tip electrode setup was used to perform a poling study at 50 °C with an applied potential difference of 15 kV increasing the duration of poling from 1 to 5 h. Corona poling is a non-contact technique ideal for the poling of ferroelectrics for biomedical applications since omitting the step of electrode deposition which can cause unwanted side effect when the ferroelectric is used as an implant. Therefore, omitting this step from the manufacturing process would not only reduce this risk but also the cost of production.[34] For these reasons, the possibility to pole ferroelectric implants without the need of electrodes is of high interest. In order to ensure uniform charges deposition which results in the effective poling of the whole sample, the needle-base distance which is approximately equal the radius of the electric field at the base of the corona poling setup, has to be set accordingly, in order for the area of electric field at the base to cover the top surface of the samples.[35] Given the fact that the samples have a cubic geometry with a top surface area of around 1.5 cm^2, the needle base distance was set at 5 cm giving an active area of 78.5 cm^2. No more than three samples were poled at the same time ensuring effective poling. The samples were placed as closer to center of the electric field as possible. The open circuit voltage coefficient (g_{33}) was calculated using the measured longitudinal piezoelectric charge coefficient (d_{33}) and permittivity values at 1 kHz using the following equation:

$$g_{33} = \frac{d_{33}}{\varepsilon_{33}^{\sigma}} \quad (2)$$

The open circuit voltage coefficient is an important parameter since it represents the electric field produced per unit stress as it can be linked with the formation of ROS in an aqueous solution. The results are plotted in **Figure 7**a,b. It can be observed that the piezoelectric performance of the composites improves with the increase in the filler concentration and the poling duration. However, increasing the poling time does not increase the polarization and hence the d_{33} and g_{33} values. In the case of piezoelectric strain coefficient, a decrease in standard deviation is observed with the increase of filler content and the increase of poling time indicating effective dipole alignment in the composite systems. Considering that PCL-30BCZT

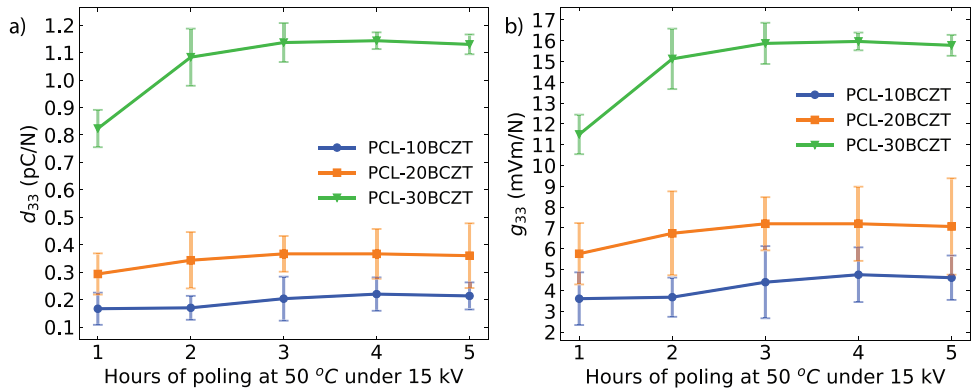

Figure 7. Poling study for evaluation of the piezoelectric of the 3D printed samples after corona discharge poling at different durations under 15 kV at 50 °C: a) Piezoelectric strain coefficient (d_{33}), b) Open circuit voltage coefficient.

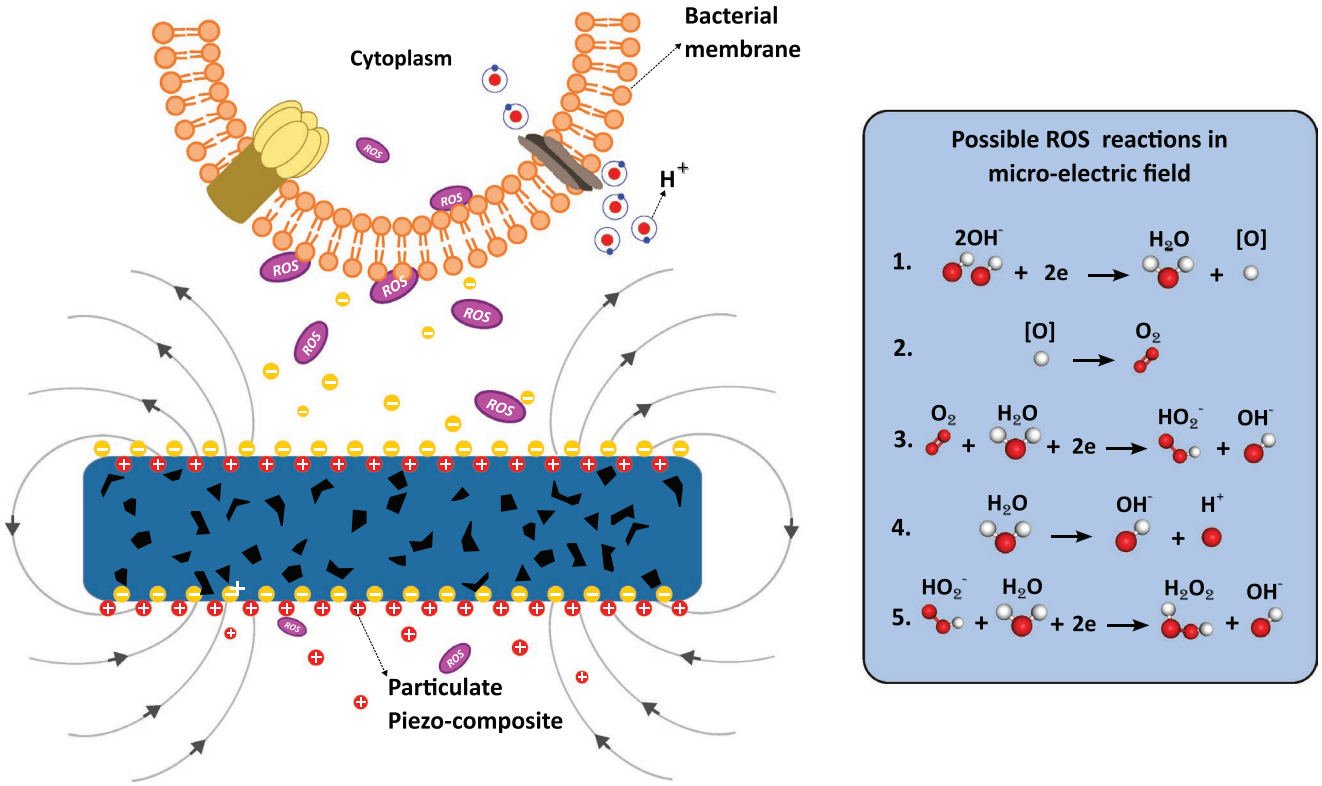

Figure 8. Schematic of the possible selective antimicrobial mechanism of the polarized 3D printed piezo-particulate PCL-BCZT composites.

samples exhibited the highest piezoelectric values, they were chosen for the antimicrobial evaluation of their surface.

The dielectric analysis shown good agreements with Yamada model. For further investigation and confirmation, the equation proposed by Yamada to estimate the piezoelectric coefficient was used.

$$d_{33(\text{eff})} = V_f \times a \times G \times d_{33(\text{BCZT})} \tag{3}$$

where V_f is the volume fraction, a is the effective poling ration, G is the local field coefficient, and d_{33} is the piezoelectric coefficient of the filler particles. The local field coefficient, which is determined by the dielectric constants of the polymer matrix and ceramic filler, can be calculated as follows:

$$G = \frac{n\left[\left(\frac{\varepsilon_{\text{BCZT}}}{\varepsilon_{PCL}} - 1\right) + n + (n-1)\left(\frac{\varepsilon_{\text{BCZT}}}{\varepsilon_{\text{PCL}}} - 1\right)V_f\right]}{\left[\left(\frac{\varepsilon_{\text{BCZT}}}{\varepsilon_{\text{PCL}}} - 1 + n\right)^2 + \left(\frac{\varepsilon_{\text{BCZT}}}{\varepsilon_{\text{PCL}}} - 1\right)\left\{(n-1)^2 - \frac{\varepsilon_{\text{BCZT}}}{\varepsilon_{\text{PCL}}}\right\}V_f\right]} \tag{4}$$

where n as previously described is a dimensionless parameter depending on the shape and orientation of the ceramic particles, ε_{PCL} and $\varepsilon_{\text{BCZT}}$ the permittivity of the matrix and ceramic filler accordingly. The model predictions are shown in Table 2 and were obtained assuming that the poling ratio was 1. Overall, the data follows the trend predicted by the model.

To observe the influence of poling on bacterial inactivation, bacterial cells were inoculated with a drop of *E. coli* at a concentration of ≈1.67×10^7 colony forming units (CFU) mL^{-1} to different surface conditions, i.e., positive side of poled, negative side of poled, the PCL (no BCZT) and a control which contained the same sized drop but instead diluted in Luri–Bertani broth and not placed on a surface. The results show that the poled surfaces can reduce the quantity of *E. coli* bacteria on the surface (Figure 9). The hypothesis is the mechanism of bacterial killing is due to ROS created due to the surface potential difference, a large surface area of the samples and finally some hydrophobic segments of the PCL matrix.[36]

After their polarization by a strong enough direct current (DC) field, the domains of the piezoelectric BCZT particles align, resulting in distribution of positive and negative charges on the surfaces. This leads to the formation of an electric field which accelerates the formation of ROS (e.g., H_2O_2, HO_2^-, and OH^-) on the cathode surface of the composites (**Figure 8**). The possible reactions that can occur are listed in the table of the Figure 8. As a result, the bacteria cultured on the positive surface are killed by ROS. Normally, when bacteria are cultured on the negative side it is less likely to be killed as the levels of ROS are lower.[15] However, if the composite is porous the ROS can travel through the composite's pores and kill the bacteria on the other surface too. Porosity also enhances the formation of ROS as the surface area is larger.

To observe the functionality of the material, the control, the positive and the negative should be compared; although a significant reduction is not observed; the ferroelectric material is decreasing the quantity of bacteria on the surface compared with just the polymer matrix (PCL). The material was exposed to a high inoculum of bacteria, to test the material in

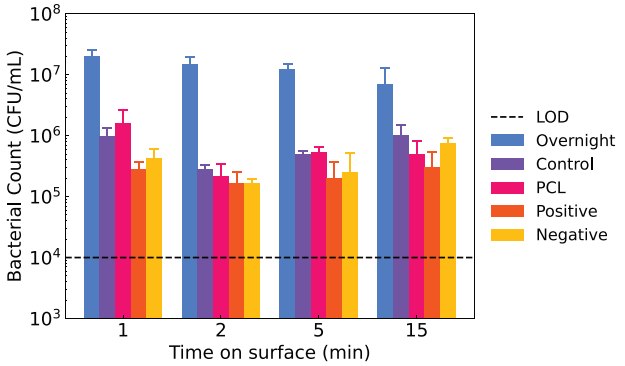

Figure 9. Survival of *E. coli* bacteria on different surfaces compared (positively charged surface of PCL-30BCZT samples negatively charged surface of PCL-30BCZT sample and polymer matrix (PCL)) with the control (not place on a surface). *E. coli* was incubated on the surface for different durations in the incubator. The quantity of bacteria remaining was determined using enumeration of the bacterial amount and the CFU/mL was calculated. (LOD: Limit of Detection).

its ability to treat very high contamination. Normally, the contaminated medical implants are only exposed to significantly lower numbers of microorganisms, often from patient's skin/mucosal membrane which then increases whilst the device is implanted.[37] The ferroelectric material shows promise in preventing these initial contamination events.

Polarized ferroelectric surfaces have recently been investigated as a sustainable method for the sterilization of surfaces. This is mainly achieved by deploying the induced electrochemical reactions by periodically mechanically/thermally or photo-exciting the ferroelectric material. However, due to the surface potential of ferroelectrics after poling, it is possible to induce the formation of ROS for short periods without any additional activation until the neutralization of the aqueous solution. Considering the state-of-the-art ferroelectrics, **Figure 9**, for antimicrobial applications, photocatalytic ferroelectrics exhibit the best performance requiring 30–60 min to reduce the number of bacteria below the limit of detection.

In this study implementing a material engineering approach, we successfully optimized the manufacturing process toward scalability and cost-effectiveness as well as the performance of ferroelectric by increasing the surface area and hence the production of ROS and by combining ferroelectric BCZT with a biocompatible polymer that facilitates bacteria reduction when the bacteria are exposed for long periods. The result is that PCL with 30 wt% BCZT seems to exhibit the best antimicrobial ferroelectric performance and needs only half of the time required by the current best antimicrobial ferroelectric system to sterilize the surface (15 min). The comparison of the antimicrobial behavior of the composites fabricated in this study with the most recent and promising ferroelectric systems used for antibacterial applications found in the literature is illustrated in **Figure 10**.

3. Conclusion

Polymer-based ferroelectric composites were discovered to exhibit antimicrobial performance on *E. coli* bacteria likely due to the release of ROS on their surface. More specifically, in this work, for the first time, PCL/BCZT composites were successfully fabricated by using a single-step extrusion-based 3D printing technology and have potential to be used as antimicrobial for biological applications. The presence of the ferroelectric ceramic powder delays the composites' degradation rate. The dielectric and piezoelectric performance improves with the increase of the ferroelectric phase in the polymer matrix. Free radicals are produced when the water molecules in the aqueous solution are microelectrolyzed by the polarized samples. The generated ROS can inactivate bacterial cells by altering their membrane properties which eventually leads in their deoxyribonucleic acid (DNA) destruction. The antimicrobial performance

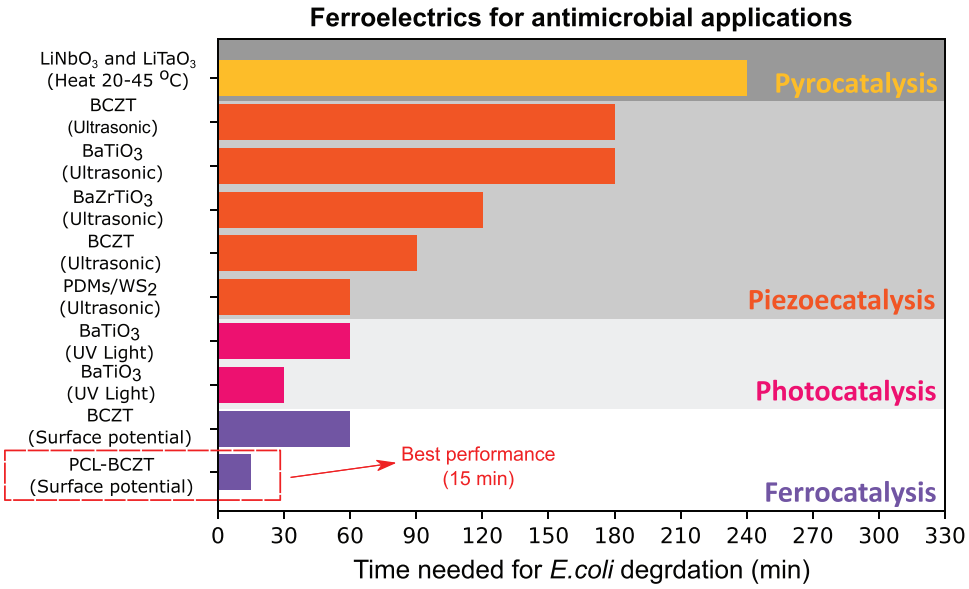

Figure 10. State of art data of ferroelectric materials for antibacterial applications.[13,17,38–42]

in the composite systems is further enhanced by the relatively large surface area of the porous samples achieved via 3D printing and the hydrophobic segments of the polymer matrix. Henceforth, based on this study is feasible to develop antibacterial and biocompatible ferroelectrics that can be used as antimicrobial surfaces or in the field of tissue engineering as the level of ROS is safe for normal mammalian cells.

4. Experimental Section

Design and Manufacturing of the 3D Printed Ferroelectric Composites: For the manufacturing of the 3D printed composites (0, 10, 20, and 30 wt%), BCZT powder was synthesized and used. The BCZT powder was synthesized by a solid-state reaction approach. In brief, highly pure barium carbonate (99%), calcium carbonate (99%), titanium dioxide (rutile) (99%), and zirconium dioxide (99%) were weighted according to the stoichiometric ratio and used for the synthesis of BCZT. The raw materials were mixed with ethanol and ball milled for 24 h. After ball milling, the powder was dried and calcined at 1200 °C for 10 h. The PCL powder used for the scaffolds manufacturing was purchased from Polyscience Europe (Germany) and has the following characteristics: M_w = 40 000–50 000, M_n = 45 000, and particle size <600 µm. The PCL and BCZT powders were weighed and homogenously mixed prior to 3D printing with 3D Bioplotter extrusion system (EnvisionTEC, Germany). More specifically, the powder mixture was loaded into metal syringe, heated to 140 °C in the 3D Bioplotter, extruded at 0.7 mm s^{-1} printing speed and 6.5 bar pressure to 3D print samples. The samples were printed with solid infill 15 × 15 × 2 mm with 5 layers using a 0.4 mm printing tip. The individual strands of material were laid adjacent to each other avoiding gaps and the alternative layering rotated by 90°. No post-processing was done.

Morphological Characteristics: The microstructure of the additively manufactured ferroelectric composites was investigated by Scanning Electron Microscopy (Hitachi FE-SEM SU5000) aiming to ensure satisfactory filler dispersion after printing. Scanning Electron Microscopy was also used for the investigation of the particle size and the morphology of the synthesized BCZT powder. The structural phase present in the powder was determined by X-ray Diffraction (XRD) measurements using CuK_a radiation (BRUKER D8-Advance, USA) in a 2θ range from 20° to 70°. Measurements of the topography parameters of the 3d printed samples were performed using a digital Keyence VHX-6000 microscope. The samples were scanned and measured using a Z20:×100 magnification lens. The surface arithmetical mean height (Sa) and maximum surface height (Sz) were given by the analysis performed through microscope's software. Finally, the porosity of the samples (in vol%) was calculated using the following equation:

$$P = \left(1 - \frac{m}{phA}\right) \times 100 \quad (5)$$

where m is the mass of the sample, ρ is the density of the samples, h is the thickness of the samples, and A is the calculated surface area. The geometrical characteristics were measured using a digital caliper micrometer and confirmed by the digital microscope.[43]

Attenuated Total Reflectance Fourier Transform Infrared Spectroscopy (ATR-FTIR): A Nicolet iS5 (Thermo Scientific, UK) system with an iD5 ATR diamond crystal window was used to perform the ATR-FTIR and examine the composition of the raw materials. The FTIR spectra for all tested materials were taken in the 450–4000 cm range.

Thermogravimetric Analysis (TGA): TGA was used to determine the thermal behavior of the extruded ferroelectric composites and evaluate the amount of BCZT in the systems. The analyses were carried out in nitrogen environment using a TGA2 METTLER TOLEDOTM instrument with a resolution of 1 µg and weighing accuracy of 0.005%. With an initial weight of around 15 mg, the extruded composites were tested at temperatures ranging from 50 to 600 °C at a rate of 10 °C min^{-1}.

Dielectric Analysis: Impedance spectroscopy was employed to analyze the electrical response of the printed ferroelectric composites. For the analysis, a 1260 A Impedance/Gain-Phase Analyzer was used. The 3d printed ferroelectric composite were tested in the frequency range from 0.1 Hz to 100 kHz at room temperature (≈25 °C), human body temperature (≈36.6 °C), and poling temperature (50 °C).

Poling Study and Piezoelectric Response: A custom made corona discharge single tip electrode setup similar to the one suggested from Waller[44] was utilized to perform a poling study at 50 °C with an applied potential difference of 15 kV increasing the duration of poling (1–5 h). In order to enable rapid ageing and allow the domains of the ferroelectric phase to stabilize the piezoelectric coefficient values (d_{33}) of the 3d printed composites were recorded the next day of the poling using a d_{33} Berlincourt piezometer supplied by Piezotest at 97 Hz. For consistency, readings were the d_{33} values were taken after 10 s of the insertion of the sample in the piezometer's clamp.

Antimicrobial Studies: To consider the impact of poling on bacterial degradation, the drop cast method was used. An overnight culture of *E. coli* ATCC 25922 was prepared using 10 mL Lurie–Bertani (LB) broth, the culture was incubated overnight at 37 °C with 200 rpm agitation. A subculture of *E. coli* was prepared at ≈1×10^7 CFU mL^{-1}. A drop (20 µL) of the subculture was dropped on the surface of the ferroelectric composites. After 1, 2, 5, 15 min the composites were submerged in 0.98 mL of PBS. The resulting mix was serially diluted and quantified using the Miles and Mirsa technique, on LB plates.[45]

Acknowledgements

Z.M.T.'s PhD research is fully supported by an Engineering and Physical Sciences Research Council (EPSRC)—DST Innovations Ltd joint studentship. R A.H.'s PhD studentship is funded by the Annette Trust and the EPSRC.

Conflict of Interest

The authors declare no conflict of interest.

Data Availability Statement

The data that support the findings of this study are available from the corresponding author upon reasonable request.

Keywords

3D printing, antimicrobial ferroelectrics, BCZT, PCL, piezoelectric scaffolds

Received: January 14, 2023
Published online: March 11, 2023

[1] D. Sun, M. Babar Shahzad, M. Li, G. Wang, D. Xu, *Mater. Technol.* **2015**, *30*, B90.
[2] E. S. Fioretta, S. E. Motta, V. Lintas, S. Loerakker, K. K. Parker, F. P. T. Baaijens, V. Falk, S. P. Hoerstrup, M. Y. Emmert, *Nat. Rev. Cardiol.* **2021**, *18*, 92.
[3] E. Mancuso, L. Shah, S. Jindal, C. Serenelli, Z. M. Tsikriteas, H. Khanbareh, A. Tirella, *Mater. Sci. Eng. C* **2021**, *126*, 112192.

[4] C. L. Romanò, H. Tsuchiya, I. Morelli, A. G. Battaglia, L. Drago, *Bone Joint Res.* **2019**, *8*, 199.
[5] K. Iskandar, J. Murugaiyan, D. Hammoudi Halat, S. E. Hage, V. Chibabhai, S. Adukkadukkam, C. Roques, L. Molinier, P. Salameh, M. Van Dongen, *Antibiotics* **2022**, *11*, 182.
[6] A. H. Holmes, L. S. P. Moore, A. Sundsfjord, M. Steinbakk, S. Regmi, A. Karkey, P. J. Guerin, L. J. V. Piddock, *Lancet* **2016**, *387*, 176.
[7] L. Cantas, S. Shah, L. Cavaco, C. Manaia, F. Walsh, M. Popowska, H. Garelick, H. Bürgmann, H. Sørum, *Front. Microbiol.* **2013**, *4*, 96.
[8] "Antimicrobial Resistance Diagnostics Market Size Report, 2030," can be found under https://www.grandviewresearch.com/industry-analysis/antimicrobial-resistance-diagnostics-market-report (accessed: November 2022).
[9] F. Siedenbiedel, J. C. Tiller, *Polymers* **2012**, *4*, 46.
[10] S. Kumar, M. Sharma, T. Frömling, R. Vaish, *J. Ind. Eng. Chem.* **2021**, *97*, 95.
[11] M. Wu, Z. Zhang, Z. Liu, J. Zhang, Y. Zhang, Y. Ding, T. Huang, D. Xiang, Z. Wang, Y. Dai, X. Wan, S. Wang, H. Qian, Q. Sun, L. Li, *Nano Today* **2021**, *37*, 101104.
[12] E. O. Carvalho, M. M. Fernandes, J. Padrao, A. Nicolau, J. Marqués-Marchán, A. Asenjo, F. M. Gama, C. Ribeiro, S. Lanceros-Mendez, *ACS Appl. Mater. Interfaces* **2019**, *11*, 27297.
[13] S. Kumar, R. Vaish, S. Powar, *J. Appl. Phys.* **2018**, *124*, 014901.
[14] A. H. Rajabi, M. Jaffe, T. L. Arinzeh, *Acta Biomater.* **2015**, *24*, 12.
[15] G. Tan, S. Wang, Y. Zhu, L. Zhou, P. Yu, X. Wang, T. He, J. Chen, C. Mao, C. Ning, *ACS Appl. Mater. Interfaces* **2016**, *8*, 24306.
[16] A. Kakekhani, S. Ismail-Beigi, *J. Mater. Chem. A* **2016**, *4*, 5235.
[17] S. Kumar, M. Sharma, S. Powar, E. N. Kabachkov, R. Vaish, *J. Eur. Ceram. Soc.* **2019**, *39*, 2915.
[18] M. Rahman, P. K. Mukherjee, in *Hybrid Polymer Composite Materials* (Eds: V. K. Thakur, M. K. Thakur, R. K. Gupta), Woodhead Publishing, Sawston, Cambridge **2017**, pp. 249–280.
[19] A. Muc, M. Barski, *Materials* **2018**, *11*, 234.
[20] Y. Wang, Y. Zhou, L. Lin, J. Corker, M. Fan, *Composites, Part A* **2020**, *139*, 106114.
[21] D. Pierantozzi, A. Scalzone, S. Jindal, L. Stīpniece, K. Šalma-Ancāne, K. Dalgarno, P. Gentile, E. Mancuso, *Compos. Sci. Technol.* **2020**, *191*, 108069.
[22] E. H. Backes, S. V. Harb, C. A. G. Beatrice, K. M. B. Shimomura, F. R. Passador, L. C. Costa, L. A. Pessan, *J. Biomed. Mater. Res., Part B* **2022**, *110*, 1479.
[23] E. Malikmammadov, T. E. Tanir, A. Kiziltay, V. Hasirci, N. Hasirci, *J. Biomater. Sci., Polym. Ed.* **2018**, *29*, 863.
[24] Y. Zhang, M. Xie, J. Roscow, C. Bowen, *Mater. Res. Bull.* **2019**, *112*, 426.
[25] S. Wu, B. Zhang, Y. Liu, X. Suo, H. Li, *Biointerphases* **2018**, *13*, 060801.
[26] A. Lu, Y. Gao, T. Jin, X. Luo, Q. Zeng, Z. Shang, *Ceram. Int.* **2020**, *46*, 6550.
[27] M. Neufurth, X. Wang, S. Wang, R. Steffen, M. Ackermann, N. D. Haep, H. C. Schröder, W. E. G. Müller, *Acta Biomater.* **2017**, *64*, 377.
[28] X. Ji, C. Wang, W. Luo, G. Chen, S. Zhang, R. Tu, Q. Shen, J. Shi, L. Zhang, *J. Sol-Gel Sci. Technol.* **2020**, *94*, 205.
[29] D. Milovac, G. Gallego Ferrer, M. Ivankovic, H. Ivankovic, *Mater. Sci. Eng., C* **2014**, *34*, 437.
[30] K. Chrissafis, D. Bikiaris, *Thermochim. Acta* **2011**, *523*, 1.
[31] V. J. Hegde, O. Gallot-Lavallée, L. Heux, in *2016 IEEE International Conference on Dielectrics (ICD)*, IEEE, Montpellier, France **2016**, pp. 293–296.
[32] A. Bagchi, S. R. K. Meka, B. N. Rao, K. Chatterjee, *Nanotechnology* **2014**, *25*, 485101.
[33] T. Yamada, T. Ueda, T. Kitayama, *J. Appl. Phys.* **1982**, *53*, 4328.
[34] M. Rotan, M. Zhuk, J. Glaum, *J. Eur. Ceram. Soc.* **2020**, *40*, 5402.
[35] S. R. Panteny, *Microstructural, Mechanical and Electrical Characterisation of Piezoelectric Particulate Composites with Dielectric Modelling*, University of Bath, Bath **2003**.
[36] X. Zhou, J. He, C. Zhou, *Polym. Chem.* **2019**, *10*, 945.
[37] C. von Eiff, B. Jansen, W. Kohnen, K. Becker, *Drugs* **2005**, *65*, 179.
[38] M. Sharma, V. P. Singh, S. Kumar, R. Vaish, *J. Appl. Phys.* **2020**, *127*, 135103.
[39] S. Masimukku, Y.-C. Hu, Z.-H. Lin, S.-W. Chan, T.-M. Chou, J. M. Wu, *Nano Energy* **2018**, *46*, 338.
[40] M. Sharma, G. Singh, R. Vaish, *J. Am. Ceram. Soc.* **2020**, *103*, 4774.
[41] J. Xu, T. Zang, D. Du, S. Kumar, M. Sharma, R. Vaish, *J. Am. Ceram. Soc.* **2021**, *104*, 1661.
[42] E. Gutmann, A. Benke, K. Gerth, H. Böttcher, E. Mehner, C. Klein, U. Krause-Buchholz, U. Bergmann, W. Pompe, D. C. Meyer, *J. Phys. Chem. C* **2012**, *116*, 5383.
[43] H. Yoon, G. Kim, *J. Pharm. Sci.* **2011**, *100*, 424.
[44] D. Waller, T. Iqbal, A. Safari, *J. Am. Ceram. Soc.* **1989**, *72*, 322.
[45] A. A. Miles, S. S. Misra, J. O. Irwin, *J. Hyg.* **1938**, *38*, 732.